

Weakly Coordinating Fluorine-Free Polysalt for Single Lithium-Ion Conductive Solid Polymer Electrolytes

Maria Martinez-Ibañez^[a] Eduardo Sanchez-Diez^[a] Lixin Qiao,^[a, b] Leire Meabe,^[a] Alexander Santiago,^[a] Haijin Zhu,^[c] Luke A. O'Dell,^[c] Javier Carrasco,^[a] Maria Forsyth,^[c] Michel Armand,^[a] and Heng Zhang^{*[a]}

A novel single lithium-ion conducting (SLIC) polymer electrolyte containing a weakly coordinating fluorine-free polysalt is presented. The polysalt, lithium poly(4-styrenesulfonyl)(dicyano)methide (LiPSDM), is conceived on the basis of a fluorine-free green chemistry, and motivated by the highly performing non-fluorinated lithium tricyanomethanide (LiTCM) salt. The electrolyte comprising LiPSDM and poly(ethylene oxide) (PEO) shows good thermal stability, decent ionic conductivity, and high lithium transference number. In stark contrast to other fluorine-free polysalts, such as, poly(4-styrenesulfonate) (LiPSS), the

replacement of SO_3^- moiety by $\text{SO}_2\text{C}^{(-)}(\text{CN})_2$ improves the flexibility of the anion and the charge delocalization, leading to an improved amorphization of PEO and an overall better performance. Moreover, solid-state nuclear magnetic resonance (NMR) measurements are performed to unravel the role of anion chemistry on the fundamental transport properties of SLICs. The present work is believed to facilitate the design of high-performance fluorine-free polymer electrolytes which are important building blocks for safe, green, and sustainable battery technologies.

1. Introduction

Lithium-ion batteries (LIBs) have experienced an exponential growth over the last three decades since their commercialization by Sony in 1990s.^[1] Nowadays, LIBs are ubiquitous in our society, dominant in small portable devices, consolidated in smart grid facilities and even able to power electric vehicles (EVs). The fight against climate change demands for the energy transition to go beyond currently implemented technology (i.e., from fossil-based to zero-carbon energy system).^[2] The use of lithium metal (Li°) as anode in the so-called lithium metal batteries (LMBs) could result in a boost of energy density in comparison to the graphite-based LIBs, due to the remarkably higher specific capacity of Li° electrode [i.e., 3860 mAh g⁻¹ (Li°) vs. 372 mAh g⁻¹ (graphite)], and thus may circumvent the shortcomings of the contemporary LIB technologies.^[3]

Recent incidents involving LIBs have brought to light the lack of safety regarding the use of flammable solvents as electrolyte and have tipped the balance in favor of safer alternatives.^[4] Consequently, several safer electrolytes have been proposed as alternatives to conventional liquid organic solvents. Among all of them, solid polymer electrolytes (SPEs), due to the easy tuning of their properties mainly by molecular engineering, are playing a leading role on the development of safe and high energy density batteries. SPEs, initially proposed by Armand^[5] in 1978 within the concept of all solid-state LMBs (ASSLMBs), have been studied in depth^[6] and are nowadays successfully applied in the automotive industry. Bolloré Bluecar[®] and Bluebus[®] are examples of the viability of the technology.^[7] However, dendrite growth and low efficiencies due to the anion concentration gradient generated by the high mobility of anionic species [i.e., low Li-ion transference number (T_{Li^+})] have restricted the large-scale implementation of LMBs technology.^[8]

SPEs, containing polar groups in the polymeric structure, are able to dissolve and dissociate the salt. In this scenario, conventional SPEs are composed of a mixture of a polymer and a salt. On one hand, polymers with low glass transitions are required to provide elevated ionic conductivities through the segmental motion of the polymeric backbone. On the other hand, anions with strong capabilities of plasticization and negative-charge delocalization are also needed to improve the ionic conductivities of SPEs. This latter approach has resulted in a golden age for perfluorinated anions, such as lithium bis(trifluoromethanesulfonyl)imide [$\text{Li}[\text{N}(\text{SO}_2\text{CF}_3)_2]$, LiTFSI] that acts as a good plasticizer and ensures high conductivity values. Yet, in most cases, the ionic conductivity is dominated by the anion, as reflected by low Li-ion transference number in PEO matrix (T_{Li^+} at ca. 0.2),^[9] which ultimately results in large polarizations

[a] Dr. M. Martinez-Ibañez,⁺ Dr. E. Sanchez-Diez,⁺ L. Qiao, Dr. L. Meabe, Dr. A. Santiago, Dr. J. Carrasco, Prof. M. Armand, Dr. H. Zhang
Centre for Cooperative Research on Alternative Energies (CIC energiGUNE)
Basque Research and Technology Alliance (BRTA),
Alava Technology Park
Albert Einstein 48, 01510 Vitoria-Gasteiz, Spain
E-mail: hzhang@cicenergigune.com

[b] L. Qiao
University of the Basque Country (UPV/EHU)
Barrio Sarriena, s/n, 48940 Leioa, Spain

[c] Dr. H. Zhu, Dr. L. A. O'Dell, Prof. M. Forsyth
Institute for Frontier Materials,
Deakin University
Geelong, VIC 3217, Australia

[+] These authors contributed equally to this work.

 Supporting information for this article is available on the WWW under
<https://doi.org/10.1002/batt.202000045>

 An invited contribution to a Special Collection on Electrolytes for Electrochemical Energy Storage

and poor cycling performance. A successful path to obtain SPEs with high selectivity in Li-ion transport is the design of single lithium-ion conductors (SLICs), where the anion is covalently attached to a polymer backbone, reducing its mobility and consequently allowing T_{Li^+} to reach values close to unity. The main advantage of this type of electrolytes is that they can support high current densities and restrict dendrite formation.

A straightforward approach to prepare SLICs relies on the strategy of grafting an anionic moiety either to a readily available monomer to later polymerize the monomer salt, or directly to a polymer leading to a polysalt. Generally, those are blended or copolymerized with poly(ethylene oxide) (PEO) in order to enhance the segmental motion to the polymeric matrix and therefore provide sufficient ionic conductivity. In this sense, lithium poly[(4-styrenesulfonyl)(trifluoromethanesulfonyl)imide] (LiPSTFSI) has received much attention as a preferred structure due to: i) feasible modification of the styrene sulfonate monomer and ii) low dissociation energy of the trifluoromethanesulfonyl imide to provide good ionic conductivity ($>10^{-5} \text{ S cm}^{-1}$ in PEO at 70°C).^[10] However, attempts to improve the performance of LiPSTFSI require extensive transformations of the anionic moiety^[11] or block-copolymerization strategies.^[12] Besides, PEO-LiPSTFSI electrolyte suffers from high interfacial resistance at the Li° electrode, emphasizing the need for further studies on SLICs. Likewise, the use of fluorine-rich pendant anions impacts severely the costs of materials and the processing of end-of-life batteries.^[13]

Thus, alternative cost-effective and more environmentally friendly starting materials are sought. In this work, the use of the dicyanomethide moiety is proposed as a readily accessible, fluorine-free anion that can lead to the corresponding styrene based polysalt, lithium poly(4-styrenesulfonyl)(dicyano)methide (LiPSDM), in a three step synthetic sequence. The analogue lithium tricyanomethanide (LiTCM) has been described as a high performing non-fluorinated salt, which has shown promising battery performance with well-defined highly ionically conductive passivation layer on Li° anode and with similar ionic

conductivity values to LiTFSI-based SPEs.^[14] The conjunction of the accessible structure of polystyrene (PS) with successfully employed $-\text{C}\equiv\text{N}$ based anionic moiety obtained by anchoring a low cost starting material as malononitrile, results in a green approach to overcome the above-mentioned limitations of LiPSTFSI. The physicochemical and electrochemical properties of the proposed LiPSDM in PEO matrix have been characterized and compared with the state-of-the-art SLICs.

2. Results and Discussion

2.1. Dissociation Energy

Figure 1 shows the optimized geometries of monomer salts and their dissociation energies (ΔE_d) computed by density functional theory (DFT) calculations. The Cartesian coordinates of the optimized geometries are collected in Table S1. As seen in Figure 1a, the bidentate coordination between the Li^+ cation and electron-donating atoms (i.e., nitrogen and oxygen) of the studied anions are energetically favorable, as supported by previous DFT studies on TFSI^- , TCM^- and other anions.^[15] In Figure 1b, the values of ΔE_d increase in the order lithium (4-styrenesulfonyl)(dicyano)methide (LiPSDM, 511 kJ mol^{-1})< lithium [(4-styrenesulfonyl)(trifluoromethanesulfonyl)imide] (LiPSTFSI, 625 kJ mol^{-1})< lithium (4-styrenesulfonate) (LiSS, 639 kJ mol^{-1})< lithium 4-vinylbenzoate (LiSC, 699 kJ mol^{-1}), suggesting several intriguing correlations between functional groups and ΔE_d : 1) the dissociation of Li^+ cations from SDM⁻ tends to be the most facile among all these four salts, which could be ascribed to the strong electron-withdrawing ability but poor chelating effect of cyano ($-\text{C}\equiv\text{N}$) groups and low donicity of the carbon center; 2) replacing oxygen atoms of carboxyl ($-\text{CO}_2^-$) group with $-\text{C}\equiv\text{N}$ group results a significant decrease of ΔE_d (i.e., 188 kJ mol^{-1}), indicating that a higher degree of negative charge delocalization is of vital importance to facilitate the dissociation of Li^+ cations; 3) the replacement of oxygen atom in SS⁻ with

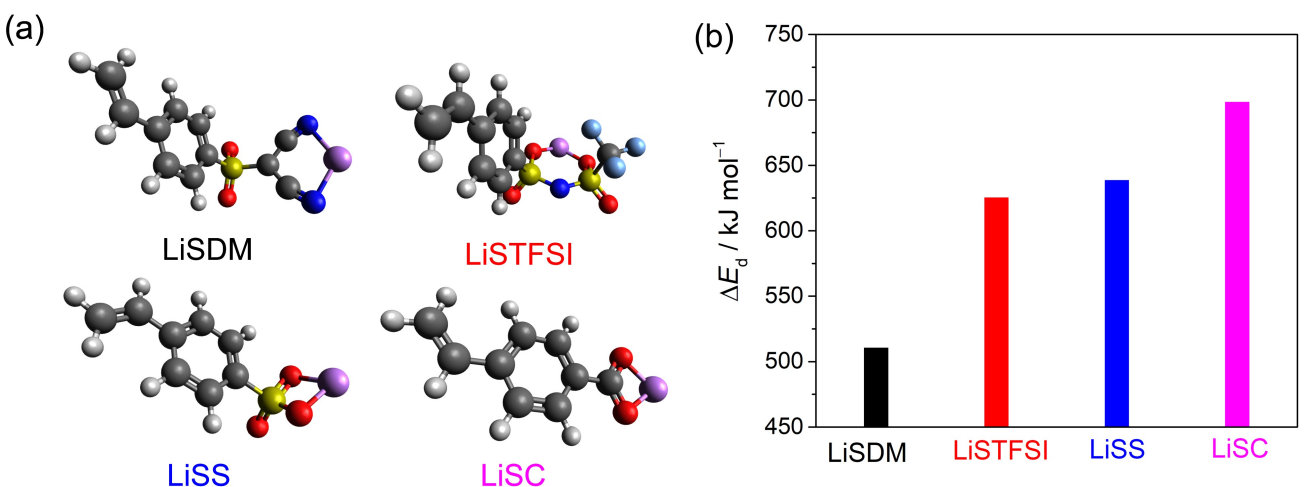


Figure 1. a) Optimized geometries and b) dissociation energies (ΔE_d) computed by DFT calculations of LiPSDM, LiPSTFSI, LiSS, and LiSC. The light gray, purple, dark blue, red, light blue, and yellow balls stand for H, Li, C, N, O, F, and S, respectively.

trifluoromethansulfonylimino ($\equiv\text{NSO}_2\text{CF}_3$) group slightly decreases the value of ΔE_d (i.e., 14 kJ mol⁻¹) but significant improvement in ionic conductivity has been observed in previous work,^[16] suggesting that the inherent flexibility of $\equiv\text{NSO}_2\text{CF}_3$ might predominate over the delocalization of negative charge in dictating the ionic transport in SLICs.

2.2. Synthesis and Structural Characterization

There are two approaches to obtain styrene based polysalts depending on the selection of starting materials. One of these is based on the use of a polystyrene sulfonate, which involves the modification of the pending arms of a polymer with a predefined molecular weight and polydispersity (PDI). Despite the advantages in terms of predictability of polymer properties, this strategy also requires arduous synthetic protocols and leads to certain level of uncertainty in the characterization steps. On the other hand, targeting a modified styrene monomer for the later polymerization process prevents incomplete functionalization of the polysalt. Therefore, a three step synthetic route to the desired LiPSDM was envisioned (Scheme 1). In a first step, commercially available sodium styrene sulfonate is subjected to a chlorination process with thionyl chloride. The introduction of the dicyanomethide moiety is accomplished in the second step taking advantage of the nucleophilicity of a cheap starting material as malononitrile in the presence of non-nucleophilic tertiary amines. In this sense, triethylamine is preferred over previously employed 1,4-diazabicyclo[2.2.2]octane (DABCO),^[17] a more complex and expensive material, leading to a clean reaction and high yields. Malononitrile as an enolate surrogate reacts smoothly with the corresponding sulfonyl chloride leading to the sulfonyl dicyanomethide anion. The intermediate undergoes subsequent acidification/lithiation steps to remove the tertiary amine and form the styrene monomer in the form of the pure lithium salt, as confirmed by nuclear magnetic resonance (NMR) in Figure

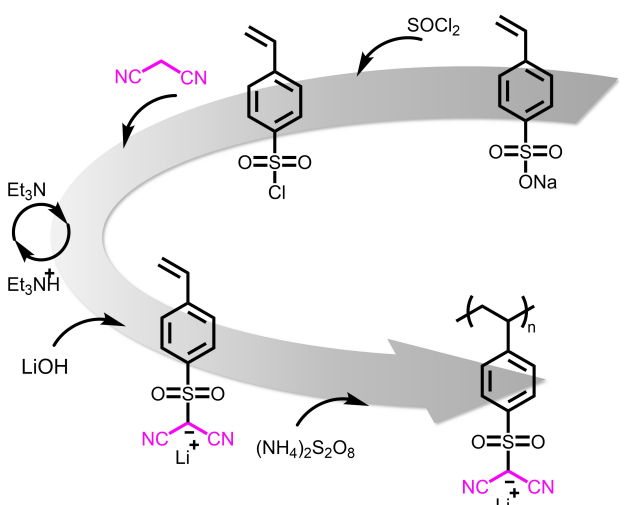
2a–b and ICP. The olefin and aromatic signals of the styrene remain distinct in both ¹H-NMR (7.8–5.4 ppm) and ¹³C-NMR (145–115 ppm), whilst new ¹³C signal at 43 ppm assigned to $-\text{C}(\text{CN})_2$ is a clear evidence of the successful grafting onto the styrene scaffold (Figure 2b). In the last step, ammonium persulfate $[(\text{NH}_4)_2\text{S}_2\text{O}_8]$ serves as initiator in a radical mediated polymerization in water for an efficient and sustainable synthesis of LiPSDM. The high degree of purity of the obtained polymer is confirmed by the absence of monomer and/or solvent in the NMR spectra. (Figures 2c–d). This approach results in a straightforward synthesis of the desired material guaranteeing a fully functionalized and lithiated polymer. The experimental details of LiPSTFSI and lithium poly(4-styrenesulfonate) (LiPSS) are given in Supporting Information (see Schemes S1–S3, Figures S1–S8)

2.3. Thermal Stability

The thermal stabilities of polysalts and their polymer blends with PEO were determined by thermogravimetric analysis (TGA). Figure 3a shows the TGA traces for the three polysalts, with no mass loss up to 350 °C. In the case of the SLICs, Figure 3b, the thermal stability is governed by the decomposition of PEO matrix, observing an abrupt mass loss at ca. 340 °C. However, PEO-LiPSS, shows a decomposition onset temperature at ca. 244 °C. This phenomenon might be due to the LiPSS salt promoting slightly earlier the decomposition of PEO, since SO_3^- is the most basic compound and ethers can be cleaved under extremely basic or acid conditions. In all the cases, the prepared SPEs offer thermal stability at temperatures much higher than the operational temperature for ASSLMBs.

2.4. Phase Transitions

The phase transition behavior of the electrolytes at a lithium concentration of 20:1 [$-\text{CH}_2\text{CH}_2\text{O}-(\text{EO})]/[\text{Li}^+$] was measured by differential scanning calorimeter (DSC) and the results are plotted in Figure 4. As depicted in Figure 4a, all samples exhibit an endothermic peak between 60 and 70 °C, attributed to the semi-crystalline nature of PEO. The addition of LiPSDM and LiPSTFSI into PEO leads to a decrease in its crystallinity compared to LiPSS, where 75% crystallinity is retained after blending. As previously reported, PS-based polymers are reluctant to mix with PEO,^[18] and for that reason the addition of these polysalts in PEO does not have the same amorphization effect as the one observed with their homologous dual-ion conducting lithium salts.^[14] However, the anion grafted to the PS backbone in these polysalt structures may promote the compatibility with PEO as is the case of LiPSTFSI and LiPSDM, where $-\text{SO}_2\text{N}^{(-)}\text{SO}_2\text{CF}_3$ and $-\text{SO}_2\text{C}^{(-)}(\text{C}\equiv\text{N})_2$ groups are free to rotate and promote the miscibility with PEO, thus decreasing the crystallinity of the polymer host. The rigid structure of $-\text{SO}_3^-$ in LiPSS, on the contrary, is not able to promote the amorphization of PEO, which may explain the obtained high crystallinity value in PEO-LiPSS blend. This



Scheme 1. Synthetic procedure of LiSDM and LiPSDM.

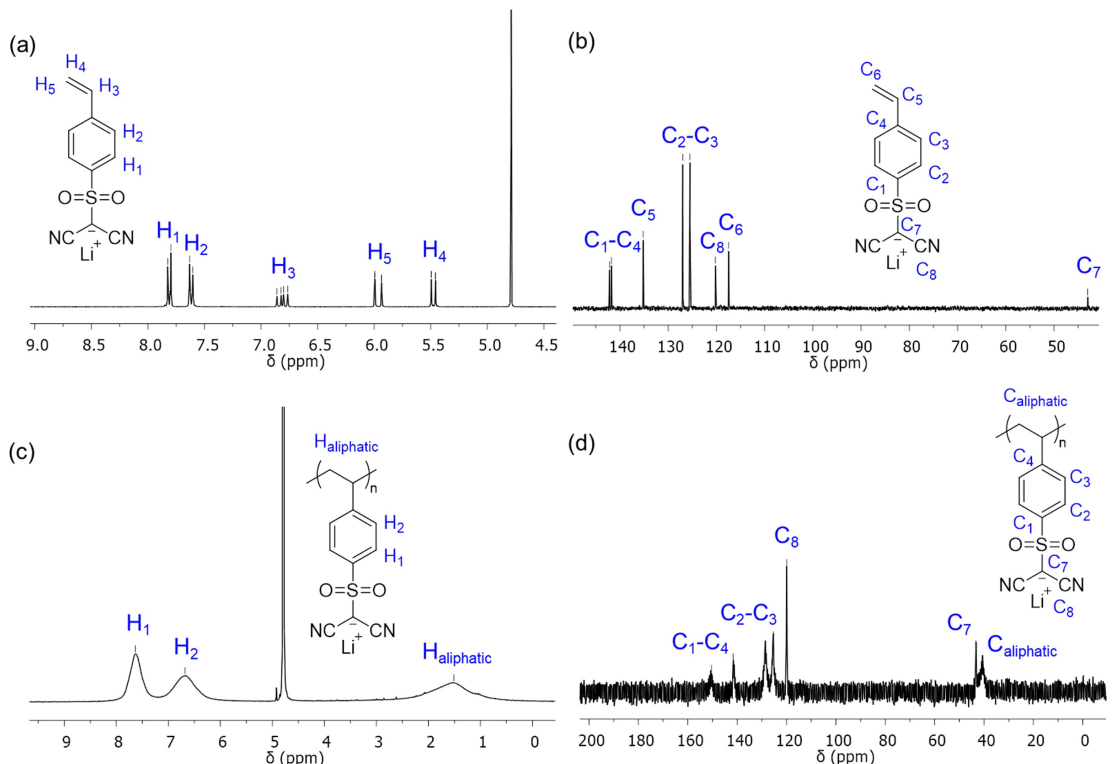


Figure 2. NMR spectra of the as-prepared LiSDM monomer: a) ^1H -NMR; b) ^{13}C -NMR; and LiPSDM polymer: c) ^1H -NMR; d) ^{13}C -NMR.

phenomenon is further confirmed by examining the zoomed area of the DSC traces for the low temperature region, Figure 4b. In the case of PEO-LiPSDM and PEO-LiPSS, the values of T_g at around -50°C are observed, attributed to the amorphous phase of neat PEO, suggesting a lower miscibility between both phases and consequently a negligible impact on the T_g value of PEO matrix. PEO-LiPSTFSI, in great contrast, shows a T_g as high as 2°C as a consequence of the better miscibility between both phases, obtaining an intermediate T_g value between those of the neat PEO and PS polymers. Thus the analysis of T_m and T_g clearly suggests i) the $-\text{SO}_2-\text{C}^{(-)}(\text{C}\equiv\text{N})_2$ moiety has better plasticizing ability compared to other non-fluorinated anions such as $-\text{SO}_3^-$ in PSS, ii) F-containing anion, $-\text{SO}_2-\text{N}^{(-)}-\text{SO}_2-\text{CF}_3$, possesses the most flexible structure offering better dissolving properties in PEO.

2.5. Ionic Conductivity and Lithium-Ion Transference Number

The ionic conductivity of different SLICs was determined by electrochemical impedance spectroscopy (EIS) in the temperature range from 40 to 100°C , as depicted in Figure 5a. The newly developed PEO-LiPSDM shows an ionic conductivity of $3.4 \times 10^{-7} \text{ S cm}^{-1}$ at 70°C , being in the typical range for SLIC-based SPEs.^[11,16] To understand the influence of the chemical nature of the covalently bonded anion on the conduction mechanism, the ionic conductivity of PEO-LiPSDM is further compared to PEO-LiPSTFSI and PEO-LiPSS, where it is found that the ionic conductivity decreases in the order of PEO-

LiPSTFSI ($4.5 \times 10^{-6} \text{ S cm}^{-1}$ at 70°C) > PEO-LiPSDM ($1.1 \times 10^{-7} \text{ S cm}^{-1}$ at 70°C) > PEO-LiPSS ($1.26 \times 10^{-8} \text{ S cm}^{-1}$ at 70°C).

On the one hand, as is typically seen in PEO-based electrolytes, PEO-LiPSDM and PEO-LiPSS show an abrupt decline in ionic conductivity values at temperatures below 70°C , ascribed to the semi-crystalline nature of PEO.^[19] The PEO-LiPSS electrolyte, on the contrary shows a different tendency independent of the melting transition of PEO. This behavior can be explained by i) the low miscibility of PSS with PEO matrices, limiting the solvation and dissociation of lithium ion in PEO, and ii) the rigid $-\text{SO}_3^-$ structures that could hardly promote the PEO chains mobility by the amorphization of the crystalline phase.

On the other hand, though the monomer of LiPSDM is predicted to have the lowest dissociation energy based on the DFT calculations, PEO-LiPSTFSI shows the highest ionic conductivity in the whole studied temperature range, close to one order of magnitude higher than PEO-LiPSDM. This is rationalized by the fact that $-\text{SO}_2-\text{N}^{(-)}-\text{SO}_2-\text{CF}_3$ (in LiPSTFSI) is more flexible than $-\text{SO}_3^-$ (in LiPSS) and $-\text{SO}_2-\text{C}^{(-)}(\text{C}\equiv\text{N})_2$ (in LiPSDM), thus effectively promoting the segmental motion of PEO chains and improving the Li conduction transport. This is supported by DSC data, Figure 4b. However, both the decreased crystallinity and higher conductivity of PEO-LiPSDM prove the better flexibility of this anion compared to other fluorine-free SLICs such as LiPSS.

Even if the ionic conductivity of this new electrolyte, PEO-LiPSDM, is lower than the values reported for its homologous dual lithium ion conducting PEO-LITCM electrolytes (ca. $1 \times$

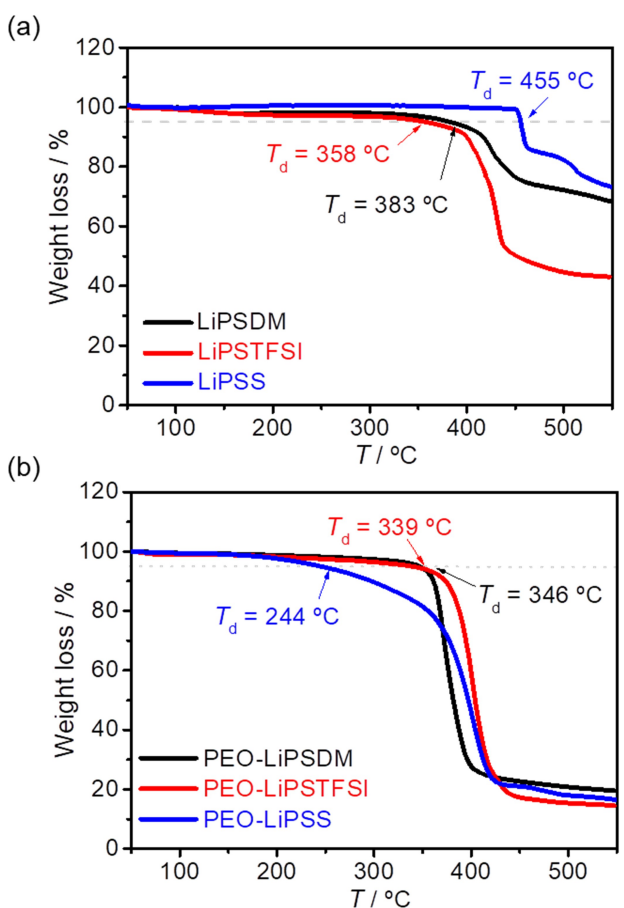


Figure 3. TGA profiles for a) the neat polysalts and b) PEO-LiPSDM, PEO-LiPSTFSI and PEO-LiPSS blends.

10^{-3} – 10^{-4} at 70 °C,^[14] it has to be considered that in this case the total ionic conductivity is mediated only by the lithium conduction, with no contribution from the counter-anion as confirmed by T_{Li^+} measurements, Figure 5b, where the value of PEO-LiPSDM is as high as 0.95 at 70 °C. In parallel, the ionic conductivity and T_{Li^+} of the LiSDM monomer blended with PEO (EO/Li=20) were also analyzed (Figure S9 and S10 in the Supporting Information), resulting in a value of $T_{\text{Li}^+}=0.41$ and a lithium conductivity ca. $1\times 10^{-4}\text{ Scm}^{-1}$ at 70 °C.

2.6. ^{7}Li Solid-State Nuclear Magnetic Resonance (SS NMR)

To gain better insights into ionic conduction mechanism and phase behavior performance, SS NMR has emerged as a key technique for understanding of the interactions among all the components of SPEs and studying of the mobility of charge carriers. In current work, ^{7}Li SS NMR was used to study the dynamics of the Li ions through spin-lattice relaxation time (T_1) and linewidth measurement over different temperatures.

The evaluation of the ^{7}Li SS NMR spectral shape can be related to the local mobility of ions.^[20] Figure 6 shows the linewidth of ^{7}Li spectra for three SLICs measured at various temperatures. Similar tendency in the linewidth is observed for

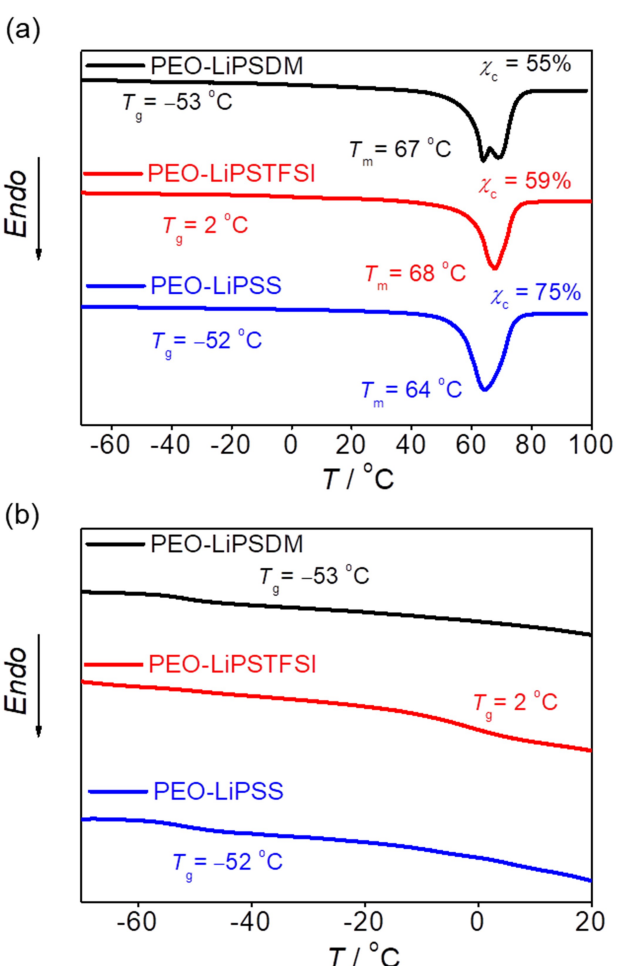


Figure 4. a) Full-range thermograms obtained by DSC of PEO-LiPSDM, PEO-LiPSTFSI and PEO-LiPSS. b) Zoomed area of the T_g region.

PEO-LiPSDM and PEO-LiPSTFSI (Figure 6a and b, respectively), with a broadening of the peak at temperatures below 60 °C, which corresponds to the melting transitions of PEO phases. Conversely, PEO-LiPSS shows a broad linewidth at all the temperature ranges (Figure 6c). Moreover, the analysis of the linewidth over temperature, summarized in Figure S11 in Supporting Information, provides a negligible dependence on the phase transitions of PEO matrix for PEO-LiPSS, while in the case of PEO-LiPSDM and PEO-LiPSTFSI, there is a steep broadening of the ^{7}Li peak at the temperatures below 60 °C, implying a slowdown of Li-ion mobility. This study is in good agreement with the results for ionic conductivity (Figure 5a), where ion conduction is clearly correlated to the melting transition of PEO. Thus, once more the $-\text{SO}_2-\text{N}^{(-)}-\text{SO}_2-\text{CF}_3$ and $-\text{SO}_2-\text{C}^{(-)}-(\text{C}\equiv\text{N})_2$ anions seem to favor the amorphization of PEO phases, promoting the lithium-ion conduction.

To gain further information related to the Li ion dynamics, ^{7}Li T_1 relaxation times were measured as a function of temperature for the three electrolytes under study, as shown in Figure 7. In all the cases, T_1 values increase when decreasing the temperature, and more interestingly the same trend as the one found in ionic conductivity is observed, where PEO-LiPSS

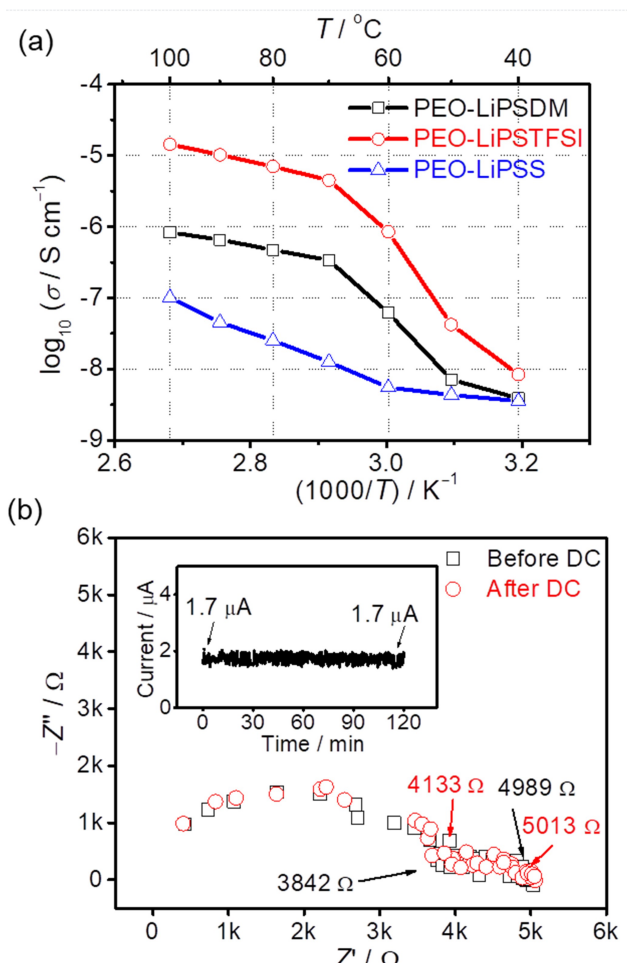


Figure 5. a) Arrhenius plot of ionic conductivity of PEO-LiPSDM, PEO-LiPSTFSI and PEO-LiPSS electrolytes. b) Impedance before and after polarization and polarization profile (inset) of the Li symmetric cells using PEO-LiPSDM electrolytes.

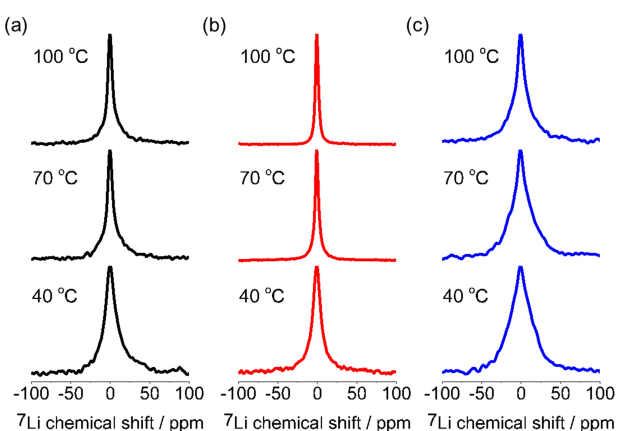


Figure 6. ^{7}Li spectra at different temperatures for a) PEO-LiPSDM, b) PEO-LiPSTFSI, and c) PEO-LiPSS.

shows the slowest dynamics. The behavior obtained for T_1 of conventional SPEs follows a parabolic tendency and can be fitted by the Bloembergen-Purcell-Pound (BPP) equation,^[21]

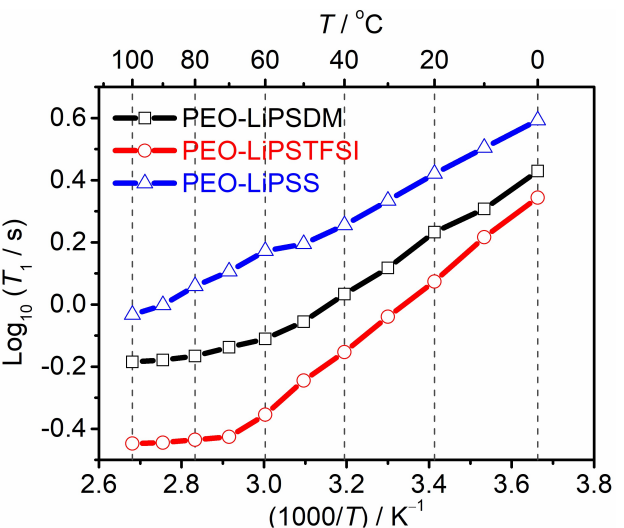


Figure 7. Arrhenius plot of $^{7}\text{Li} T_1$ relaxation time of PEO-LiPSDM, PEO-LiPSTFSI, and PEO-LiPSS.

however, in this case the ^{7}Li spin-lattice relaxation does not show any temperature dependency at high temperatures for PEO-LiPSTFSI and PEO-LiPSDM. Moreover, PEO-LiPSS shows a linear dependence with temperature, preventing the application of the BPP model in an accurate way. Comparing all the data, the two main observations that can be extracted from T_1 analysis are: i) the T_1 minimum is at a lower temperature for PEO-LiPSTFSI (i.e., 60–70 °C) which indicates faster local dynamics for the lithium than in the other SLICs, likewise, the T_1 minimum for PEO-LiPSS tends to be higher (i.e., above the upper limit of measured temperatures, >100 °C), suggesting slower local dynamics than PEO-LiPSDM; ii) the minimum T_1 value is shorter for PEO-LiPSTFSI than for PEO-LiPSDM [i.e., $T_1 = 0.36$ s (PEO-LiPSTFSI) vs. $T_1 = 0.65$ s (PEO-LiPSDM)], reflecting the different coordination environments for the lithium.

Thus, the findings obtained by SS NMR allowed to understand the local dynamics of the different SLICs, and further supports the performance observed by ionic conductivity measurements (Figure 5a), where PEO-LiPSS shows the lowest conduction and local mobility. Moreover, same curve shape is obtained where PEO-LiPSDM and PEO-LiPSTFSI show a steep decay at temperatures below 70 °C. The overall low dependence on the performance for PEO-LiPSS with the T_m of PEO might be ascribed as previously discussed to a more rigid nature of the LiPSS matrix, and an inferior miscibility between LiPSS and PEO, leading to impeded Li ion motion and transport.

3. Conclusions

In summary, we report a novel fluorine-free polymer containing a weakly coordinating anion with dicyanomethyl moiety grafted to polystyrene backbones (LiPSDM). LiPSDM has lower dissociation energy compared to LiPSS and LiPSTFSI due to the strong electron-withdrawing and poorer chelating effect of

$\text{--C}\equiv\text{N}$ group. The neat salt LiPSDM shows good thermal stability ($\sim 380^\circ\text{C}$) and the resulting electrolyte using PEO as a polymer matrix is also stable up to 330°C . Interestingly, the PEO-LiPSDM electrolyte possesses decent ionic conductivity at elevated temperature (ca. 10^{-7} Scm^{-1} , 70°C) with single Li-ion conductive nature ($T_{\text{Li}^+} = 0.95$ at 70°C) due to the good compatibility between LiPSDM and PEO attributed to sulfonyl dicyanomethyl moiety and improved plasticizing ability of LiPSDM, compared to other non-fluorinated anions. A deep study on the local dynamics of Li ions via SS NMR further reinforces the results obtained by DSC and conductivity measurements, where Li^+ species are relatively mobile in PEO-LiPSDM, particularly, after the melting transition of PEO phase. Therefore, we anticipate that sulfonyl dicyanomethyl moiety could be a potential alternative to fluorinated functional groups in building fluorine-free, highly conductive SLICs which are considered to be vital for developing green, safe, and high-performance rechargeable batteries.

Experimental Section

Theoretical methods

DFT calculations are based on the Becke's three parameters (B3) exchange functional along with the Lee-Yang-Parr (LYP) non-local correlation functional (B3LYP),^[22] as implemented in the numeric atom-centered basis set all-electron code FHI-aims.^[23] Using the open-source molecular editor and visualizer Avogadro,^[24] several plausible initial geometries were first constructed for each LiSDM, LiSTFSI, LiSS, LiSC and monomers; then full relaxation of the atomic structures was carried out with FHI-aims to identify the most stable configuration in each case. ΔE_d was computed as $\Delta E_d = E(\text{A}^-) + E(\text{Li}^+) - E(\text{LiA})$, where $E(\text{A}^-)$, $E(\text{Li}^+)$, and $E(\text{LiA})$ are the total gas-phase energies of the negatively charged anion, a positively charged Li atom, and the corresponding neutral monomer, respectively.

Materials

Thionyl chloride (Sigma-Aldrich), 4-tert-butylcatechol (TBC, Sigma-Aldrich), anhydrous dimethylformamide (DMF, Sigma-Aldrich), anhydrous acetonitrile (Scharlab), triethylamine (Sigma-Aldrich), diethyl ether (DEE, Sigma-Aldrich), methanol (Scharlab), dichloromethane (DCM, Scharlab), sodium bicarbonate (Sigma-Aldrich), ammonium persulfate (APS, Sigma-Aldrich), hydrochloric acid (Scharlab), sulfuric acid (Scharlab), malononitrile (Sigma-Aldrich) and poly(ethylene oxide) (PEO, $M_w = 5 \times 10^6 \text{ g mol}^{-1}$, Sigma-Aldrich) were used as purchased. Sodium *p*-styrene sulfonate (Sigma-Aldrich), trifluoromethanesulfonamide (Provisco), lithium hydroxide LiOH (Sigma-Aldrich) were dried before use.

Chemical structure characterization

(a) Nuclear magnetic resonance spectroscopy [NMR, Bruker 300 Ultrashield (300 MHz for ^1H , 75.5 MHz for ^{13}C and 283 MHz for ^{19}F)] was used to characterize the structure of synthesized monomer and polymer. Chemical shifts (δ) are reported in ppm relative to residual solvent signals (DMSO, 2.50 ppm, H_2O 4.79 ppm for $^1\text{H-NMR}$ and DMSO 39.52 ppm for $^{13}\text{C-NMR}$) or internal reference (CCl_3F for $^{19}\text{F-NMR}$). The following abbreviations are used to indicate the multiplicity in ^1H NMR spectra: s, singlet; d, doublet; t, triplet; q, quartet; m, multiplet; bs, broad signal. (b) Inductively

coupled plasma optical emission spectroscopy (ICP-OES Horiba Ultima) was used to confirm the lithiation of the monomer and the absence of other type of cation.

Synthesis of lithium (4-styrenesulfonyl)(dicyano)methide (LiSDM)

LiSDM was prepared using a modified procedure to the one outlined by Meziane et al.^[25] as shown in Scheme S1b. Sodium *p*-styrenesulfonate (20 g, 1 eq., 96.9 mmol) was added slowly over a solution of thionyl chloride (15 mL, 2.3 eq., 223.1 mmol) and TBC (244 mg, 1.5 mol%, 1.5 mmol) in DMF (40 mL) under argon atmosphere at 0°C . The reaction was allowed to reach room temperature and stirred for further 16 h. Excess of thionyl chloride was quenched with water and the mixture was extracted with diethyl ether ($3 \times 50 \text{ mL}$) and collected organics were sequentially washed with deionized (DI) water ($1 \times 30 \text{ mL}$) and brine solution ($1 \times 30 \text{ mL}$). Solvent was removed in vacuo to yield 4-styrene sulfonyl chloride (1b) as yellowish oil (12 g, 59.3 mmol, 61% yield). Then, to a solution of malononitrile (3.5 g, 1 eq., 52.5 mmol) in anhydrous acetonitrile (34 mL) a solution of 4-styrene sulfonyl chloride (12 g, 1.1 eq., 59.3 mmol) in anhydrous acetonitrile (34 mL) was added under argon protection followed by triethylamine (38 mL, 5.1 eq., 268.7 mmol) at 0°C . The reaction was stirred at room temperature and monitored by $^1\text{H-NMR}$. Solvent was removed in vacuo and the crude was dissolved in a LiOH (4 eq.) aqueous solution. The mixture was stirred for 1 h until completely homogeneous solution was obtained, prior to be acidified with H_2SO_4 (conc.) (7 eq.). The aqueous solution was extracted with DCM ($3 \times 80 \text{ mL}$). Organics were collected and solvent was removed in vacuo to yield a pale yellow powder corresponding to (4-styrenesulfonyl)malononitrile (2a) that was used without further purification. Finally, 2a was taken up in DI water (80 mL) and LiOH (5.0 g, 4 eq., 210 mmol) was added. The reaction mixture was stirred overnight. Excess of LiOH was removed by filtration after water evaporation and acetonitrile extraction. Solvent was removed in vacuo yielding the corresponding lithium salt, LiSDM (2b), as a pale yellow solid (11.0 g, 46.2 mmol, 88% yield). $^1\text{H NMR}$ (300 MHz, D_2O , ppm): $\delta = 7.81$ (d, $J = 8.6 \text{ Hz}$, 2H), $\delta = 7.62$ (d, $J = 8.5 \text{ Hz}$, 2H), 6.81 (dd, $J = 17.7, 11.0 \text{ Hz}$, 1H), $\delta = 5.97$ (dd, $J = 17.7, 0.5 \text{ Hz}$, 1H), 5.48 (dd, $J = 11.0, 0.5 \text{ Hz}$, 1H). $^{13}\text{C NMR}$ (75 MHz, D_2O , ppm): $\delta = 142.1, 141.7, 135.5, 127.0, 125.5, 120.2, 117.5, 43$. The NMR spectra are shown in Figure 2a and b. ICP: Lithiation degree = $98 \pm 3\%$.

Synthesis of lithium poly[(4-styrenesulfonyl)(dicyano)methide] (LiPSDM)

The synthetic route of LiPSDM is shown in Scheme S1b. A solution of LiSDM (6 g, 1 eq., 25.2 mmol) and APS (120 mg, 0.02 eq., 0.53 mmol) in DI water (120 mL) was subjected to three freeze-pump-thaw cycles. Then, subjected to an Ar atmosphere and set into a preheated bath at 80°C . The reaction mixture was stirred for 19 h. Solvent was removed under reduced pressure and the resulting waxy solid was repeatedly washed with hot THF:DI water (20:1) solution. Solution was removed and the obtained yellow solid was dried under reduced pressure. (5.2 g, 85% yield). $^1\text{H NMR}$ (300 MHz, D_2O , ppm): $\delta = 7.63$ (bs, 2H), $\delta = 6.68$ (bs, 2H), 1.51 (bs, 3H). $^{13}\text{C NMR}$ (75 MHz, D_2O , ppm): $\delta = 150.4, 141.6, 128.7, 125.3, 119.9, 43.3, 40.8$. The NMR spectra are shown in Figure 1c and d.

Preparation of polymer electrolytes

Three different electrolytes were prepared by conventional solvent-casting method, consisting of blends of PEO with the SLICs: PEO-

LiPSDM, PEO-LiPSTFSI and PEO-LiPSS. The salt concentration was kept constant in all the cases at 20:1 (the molar ratio of $-\text{CH}_2\text{CH}_2\text{O}-([\text{EO}])/([\text{Li}^+])$). PEO was dissolved into a mixture of acetonitrile and distilled water (50:50) and then a pre-determined amount of polysalt was added. After casting and solvent evaporation, electrolytes were dried under dynamic vacuum applying a ramp of temperatures from 50 to 100 °C for 24 h. Membranes with an average thickness of 150 µm were obtained by hot-pressing.

Thermal characterization

Thermogravimetric analysis (TGA) was carried out on a NETZSCH simultaneous thermal analyzer (STA 449 F3 Jupiter®) under argon flow heating from room temperature up to 550 °C. The phase transition behavior of the electrolytes was measured on a differential scanning calorimeter (DSC, Q2000, TA Instruments) from -80 °C to 100 °C. All the measurements were carried out at a heating rate of 10 °C min⁻¹. The crystalline fraction (χ_c) of the polymer electrolytes was calculated by Equation (1) below:

$$\chi_c = \frac{\Delta H_m}{\Delta H_{\text{PEO}} \times f_{\text{PEO}}} \times 100 \quad (1)$$

where ΔH_m is the melting enthalpy of electrolyte, ΔH_{PEO} is the value of 196.4 J g⁻¹ for PEO perfect crystals reported in literature for the melting enthalpy of 100% crystalline PEO,^[26] and f_{PEO} is the PEO weight fraction in the electrolyte.

Ionic conductivity

The ionic conductivity was measured by electrochemical impedance spectroscopy (EIS) on a BT lab® potentiostat (Bio-Logic Science Instruments) in the frequency range from 10⁴ to 10⁻¹ Hz with a signal amplitude of 10 mV, at a variable temperature from 40 to 100 °C. CR2032 type coin cells were assembled using two stainless steel (SS) blocking electrodes (SS|SPEs|SS) in an Ar filled glovebox ($\text{O}_2 < 0.1$ ppm, $\text{H}_2\text{O} < 0.1$ ppm) for the measurement.

Lithium-ion transference number

The lithium-ion transference number (T_{Li}^+) of SLICs was measured by a combined measurement of AC impedance and DC polarization using a symmetric $\text{Li}^\circ|\text{SPE}|\text{Li}^\circ$ cell at 70 °C VMP3 potentiostat (Biologic) at 70 °C. The impedance spectra of the cell were recorded in the frequency range from 10⁻² to 10⁶ Hz with an oscillation voltage of 10 mV, before and after the DC polarization. The value of T_{Li}^+ was calculated by Bruce and Vincent method,^[27] by applying Equation (2):

$$T_{\text{Li}}^+ = \frac{I_s R_b^s (\Delta V - I_0 R_i^0)}{I_0 R_b^0 (\Delta V - I_s R_i^s)} \quad (2)$$

Wherein, I_0 and I_s are the respective initial and steady-state currents, R_b^0 and R_b^s are the respective initial and final resistances of the bulk electrolytes, R_i^0 and R_i^s are the respective initial and final interfacial resistances of the Li° electrode/electrolyte interface and ΔV is the applied DC voltage.

⁷Li solid-state nuclear magnetic resonance (SS NMR)

Solid-state ⁷Li NMR spectra were recorded on a 300 MHz Bruker Avance III wide-bore spectrometer equipped with a 4 mm H/F-X double resonance MAS probe. Samples were packed and sealed in

a 4 mm NMR MAS rotor in an argon-filled glovebox. Temperature dependency of the ⁷Li linewidth was determined as the full width at half maximum of the peaks. ⁷Li spin-lattice relaxation time (T_1) was measured using inversion recovery experiments at temperatures ranging from 0 to 100 °C.

Acknowledgements

This work was supported by the Ministerio de Economía y Competitividad (MINECO) of the Spanish Government through Proyectos I+D Retos program (ENE2015-64907C2-1-R and ENE2016-81020-R grants) and the Basque Government through the ELKARTEK-2016 program. M.M.I. is thankful to the Spanish Government for the José Castillejo mobility program (CAS19/00309), H.Z. is grateful to the Basque Government for the Berriketu program (1-AFW-2017-2) and L.Q. thanks the financial support from Chinese Scholarship Council (no. 201808370162). M.F. is indebted to the financial support of Australia-India Strategic Research Fund (AISRF 48515) and the Ikerbasque Foundation in the Basque Country, Spain. We are also grateful for computer resources to SGI/IZOSGIker UPV/EHU (Arina cluster).

Conflict of Interest

The authors declare no conflict of interest.

Keywords: lithium batteries · solid polymer electrolytes · single lithium-ion conductor · lithium poly(4-styrenesulfonyl)(dicyano)methide

- [1] a) J. B. Goodenough, K.-S. Park, *J. Am. Chem. Soc.* **2013**, *135*, 1167–1176; b) J. B. Goodenough, *Nat. Electron.* **2018**, *1*, 204–204.
- [2] D. Gielen, F. Boshell, D. Saygin, M. D. Bazilian, N. Wagner, R. Gorini, *Energy Strateg. Rev.* **2019**, *24*, 38–50.
- [3] a) J. Schnell, T. Günther, T. Knoche, C. Vieider, L. Köhler, A. Just, M. Keller, S. Passerini, G. Reinhart, *J. Power Sources* **2018**, *382*, 160–175; b) D. Lin, Y. Liu, Y. Cui, *Nat. Nanotechnol.* **2017**, *12*, 194; c) X. Judez, G. G. Eshetu, C. Li, L. M. Rodriguez-Martinez, H. Zhang, M. Armand, *Joule* **2018**, *2*, 2208–2224; d) P. G. Bruce, S. A. Freunberger, L. J. Hardwick, J.-M. Tarascon, *Nat. Mater.* **2012**, *11*, 19–29; e) J. W. Choi, D. Aurbach, *Nat. Rev. Mater.* **2016**, *1*, 1–16.
- [4] https://www.faa.gov/hazmat/resources/lithium_batteries/.
- [5] M. Armand, J. Chabagno, M. Duclot, in *Proceedings of 2nd International Conference on Solid Electrolytes*, St. Andrews, Scotland, 1978.
- [6] a) M. Forsyth, L. Porcarelli, X. Wang, N. Goujon, D. Mecerreyes, *Acc. Chem. Res.* **2019**, *52*, 686–694; b) D. T. Hallinan Jr, N. P. Balsara, *Annu. Rev. Mater. Res.* **2013**, *43*, 503–525; c) J. Mindemark, M. J. Lacey, T. Bowden, D. Brandell, *Prog. Polym. Sci.* **2018**, *81*, 114–143; d) H. Zhang, C. Li, M. Piszcza, E. Coya, T. Rojo, L. M. Rodriguez-Martinez, M. Armand, Z. Zhou, *Chem. Soc. Rev.* **2017**, *46*, 797–815.
- [7] <https://www.bollore.com/en/activites-et-participations-2/stockage-de-lithium-solide-et-systemes-blue-applications/>.
- [8] a) X.-B. Cheng, R. Zhang, C.-Z. Zhao, Q. Zhang, *Chem. Rev.* **2017**, *117*, 10403–10473; b) H. Zhang, G. G. Eshetu, X. Judez, C. Li, L. M. Rodriguez-Martinez, M. Armand, *Angew. Chem. Int. Ed.* **2018**, *57*, 15002–15027; c) W. Xu, J. Wang, F. Ding, X. Chen, E. Nasibulin, Y. Zhang, J.-G. Zhang, *Energy Environ. Sci.* **2014**, *7*, 513–537.
- [9] a) H. Zhang, C. Liu, L. Zheng, F. Xu, W. Feng, H. Li, X. Huang, M. Armand, J. Nie, Z. Zhou, *Electrochim. Acta* **2014**, *133*, 529–538; b) J.-N. Chazalviel, *Phys. Rev. A* **1990**, *42*, 7355; c) M. Doyle, T. F. Fuller, J. Newman, *Electrochim. Acta* **1994**, *39*, 2073–2081.

- [10] a) S. Feng, D. Shi, F. Liu, L. Zheng, J. Nie, W. Feng, X. Huang, M. Armand, Z. Zhou, *Electrochim. Acta* **2013**, *93*, 254–263; b) N. Bloembergen, E. M. Purcell, R. V. Pound, *Phys. Rev.* **1948**, *73*, 679.
- [11] Q. Ma, Y. Xia, W. Feng, J. Nie, Y.-S. Hu, H. Li, X. Huang, L. Chen, M. Armand, Z.-B. Zhou, *RSC Adv.* **2016**, *6*, 32454–32461.
- [12] a) R. Bouchet, S. Maria, R. Meziane, A. Aboulaich, L. Liénafa, J.-P. Bonnet, T. N. Phan, D. Bertin, D. Gigmes, D. Devaux, *Nat. Mater.* **2013**, *12*, 452–457; b) D. Devaux, L. Liénafa, E. Beaudoïn, S. Maria, T. N. T. Phan, D. Gigmes, E. Giroud, P. Davidson, R. Bouchet, *Electrochim. Acta* **2018**, *269*, 250–261.
- [13] a) G. Siegemund, W. Schwertfeger, A. Feiring, B. Smart, F. Behr, H. Vogel, B. McKusick, *Ullmann's Encyclopedia of Industrial Chemistry* **2000**; b) L. Conte, G. Gambaretto, G. Caporiccio, F. Alessandrini, S. Passerini, *J. Fluorine Chem.* **2004**, *125*, 243–252; c) H. Zhang, W. Feng, J. Nie, Z. Zhou, *J. Fluorine Chem.* **2015**, *174*, 49–61.
- [14] H. Zhang, X. Judez, A. Santiago, M. Martinez-Ibañez, M. Á. Muñoz-Márquez, J. Carrasco, C. Li, G. G. Eshetu, M. Armand, *Adv. Energy Mater.* **2019**, *9*, 1900763.
- [15] a) H. Zhang, O. Arcelus, J. Carrasco, *Electrochim. Acta* **2018**, *280*, 290–299; b) H. Zhang, F. Chen, O. Lakuntza, U. Oteo, L. Qiao, M. Martinez-Ibanez, H. Zhu, J. Carrasco, M. Forsyth, M. Armand, *Angew. Chem. Int. Ed.* **2019**, *58*, 12070–12075; c) H. Zhang, U. Oteo, H. Zhu, X. Judez, M. Martinez-Ibanez, I. Aldalur, E. Sanchez-Diez, C. Li, J. Carrasco, M. Forsyth, M. Armand, *Angew. Chem. Int. Ed.* **2019**, *58*, 7829–7834.
- [16] Q. Ma, H. Zhang, C. Zhou, L. Zheng, P. Cheng, J. Nie, W. Feng, Y. S. Hu, H. Li, X. Huang, L. Chen, M. Armand, Z. Zhou, *Angew. Chem. Int. Ed.* **2016**, *55*, 2521–2525.
- [17] M. Armand, Y. Choquette, M. Gauthier, C. Michot, Eur. Patent, EP 0 850 921 A1, **1998**.
- [18] a) E. Yilmaz, O. Yilmaz, H. Caner, *Eur. Polym. J.* **1996**, *32*, 927–933; b) I. Aldalur, M. Martinez-Ibañez, M. Piszcza, H. Zhang, M. Armand, *Batteries & Supercaps* **2018**, *1*, 149–159; *Supercaps* **2018**, *1*, 149–159.
- [19] a) X. Judez, M. Piszcza, E. Coya, C. Li, I. Aldalur, U. Oteo, Y. Zhang, W. Zhang, L. M. Rodriguez-Martinez, H. Zhang, M. Armand, *Solid State Ionics* **2018**, *318*, 95–101; b) G. G. Eshetu, X. Judez, C. Li, M. Martinez-Ibanez, I. Gracia, O. Bondarchuk, J. Carrasco, L. M. Rodriguez-Martinez, H. Zhang, M. Armand, *J. Am. Chem. Soc.* **2018**, *140*, 9921–9933.
- [20] a) J.-D. Jeon, S.-Y. Kwak, *Macromolecules* **2006**, *39*, 8027–8034; b) N. Lago, O. Garcia-Calvo, J. M. Lopez del Amo, T. Rojo, M. Armand, *ChemSusChem* **2015**, *8*, 3039–3043.
- [21] L. Meabe, T. V. Huynh, N. Lago, H. Sardon, C. Li, L. A. O'Dell, M. Armand, M. Forsyth, D. Mecerreyes, *Electrochim. Acta* **2018**, *264*, 367–375.
- [22] a) A. D. Becke, *J. Chem. Phys.* **1993**, *98*, 1372–1377; b) C. Lee, W. Yang, R. G. Parr, *Phys. Rev. B* **1988**, *37*, 785.
- [23] a) V. Havu, V. Blum, P. Havu, M. Scheffler, *J. Comput. Phys.* **2009**, *228*, 8367–8379; b) V. Blum, R. Gehrke, F. Hanke, P. Havu, V. Havu, X. Ren, K. Reuter, M. Scheffler, *Comput. Phys. Commun.* **2009**, *180*, 2175–2196.
- [24] M. D. Hanwell, D. E. Curtis, D. C. Lonie, T. Vandermeersch, E. Zurek, G. R. Hutchison, *J. Cheminf.* **2012**, *4*, 17.
- [25] R. Meziane, J.-P. Bonnet, M. Courty, K. Djellab, M. Armand, *Electrochim. Acta* **2011**, *57*, 14–19.
- [26] N. A. Stolwijk, C. Heddier, M. Reschke, M. Wiencierz, J. Bokeloh, G. Wilde, *Macromolecules* **2013**, *46*, 8580–8588.
- [27] a) J. Evans, C. A. Vincent, P. G. Bruce, *Polymer* **1987**, *28*, 2324–2328; b) K. Abraham, Z. Jiang, B. Carroll, *Chem. Mater.* **1997**, *9*, 1978–1988.

Manuscript received: February 27, 2020

Revised manuscript received: April 2, 2020

Accepted manuscript online: April 28, 2020

Version of record online: May 13, 2020